Japanese Journal of Applied Physics

The Japan Society of Applied Physics

REGULAR PAPER

Design and characteristics of reflectivity tunable mirror with MZI and loop waveguide on SOI

To cite this article: Yutaka Makihara *et al* 2022 *Jpn. J. Appl. Phys.* **61** SC1036

View the article online for updates and enhancements.

You may also like

- Performance Simulation of Tubular Segmented-in-Series SOFC Using Simplified Equivalent Circuit
Shun Yoshida, Tadashi Tanaka and Yoshitaka Inui
- *(Invited)* Potential of Double Network Gel as a Tribological Material Realizing Low Friction in Water
Koki Kanda and Koshi Adachi
- Analysis of the Effect of Surface Diffusion on Effective Diffusivity of Oxygen in Catalyst Layer By Direct Simulation Monte Carlo
Tomoki Hori, Takuya Mabuchi, Ikuya Kinefuchi et al.

This content was downloaded from IP address 131.112.125.217 on 25/04/2022 at 13:14

Japanese Journal of Applied Physics **61**, SC1036 (2022) **REGULAR PAPER**
https://doi.org/**10.35848/1347-4065/ac465b**

Design and characteristics of reflectivity tunable mirror with MZI and loop waveguide on SOI

Yutaka Makihara[1], Moataz Eissa[1], Tomohiro Amemiya[1,2], and Nobuhiko Nishiyama[1,2*]

[1]*Department of Electrical and Electronic Engineering, Tokyo Institute of Technology, Tokyo 152-8550, Japan*
[2]*Institute of Innovative Research (IIR), Tokyo Institute of Technology, Tokyo 152-8552, Japan*

*E-mail: nishiyama@ee.e.titech.ac.jp

Received October 5, 2021; revised December 20, 2021; accepted December 23, 2021; published online February 16, 2022

To achieve a reconfigurable photonic integrated circuit with active elements, we proposed a reflectivity tunable mirror constructed using a Mach–Zehnder interferometer (MZI) with a micro heater and loop waveguide on a silicon photonics platform. In this paper, the principle of the operation, design, fabrication, and measurement results of the mirror are presented. In theory, the phase shift dependence of the mirror relies on the coupling coefficient of the directional couplers of the MZI. When the coupling coefficient κ^2 was 0.5 and 0.15, the reflection could be turned on and off with a phase shift of $\pi/2$ and π, respectively. The reflection power of the fabricated mirror on the silicon on insulator substrate was changed by more than 20 dB by a phase shift. In addition, it was demonstrated that the phase shift dependence of the mirror changes with the coupling coefficient of the fabricated devices. © 2022 The Japan Society of Applied Physics

1. Introduction

Photonic integrated circuits (PICs) on silicon photonics platforms are being used in various applications such as optical communication and optical sensing.[1,2] These PICs are typically designed specifically for particular applications. However, in terms of volume manufacturing and development costs, it is better to use the same PICs for various applications. Especially for silicon photonics, a complementary metal-oxide-semiconductor (CMOS) foundry that can fabricate a large quantity of wafers is advantageous. If the volume is small, the cost per wafer increases. This situation is similar to application specific integrated circuit and field programmable gate array (FPGA) in electric circuits. Therefore, photonic FPGA or reconfigurable photonic integrated circuits (R-PICs) have been proposed in photonic circuits.[3–5] These circuits can change the functions by programming the setup ports in the same chip after fabrication.

As an example, the circuits that comprise many Mach–Zehnder interferometers (MZIs) for expressing matrices that imitate a neural network have been studied.[6–11] Recirculation meshes, which can change the route of the waveguide by using a mesh structure that includes 2×2 gates capable of tuning cross and bar states, have been studied.[12–14] These circuits can reconfigure their structures and functions. In addition, reconfigurable photonic circuits using micro electromechanical systems have been studied.[15–17]

Such large-scale PICs have been realized using silicon photonics. Owing to the high refractive index difference between the core Si and the clad SiO_2, high optical confinement can be achieved; moreover, miniaturization and mass production is possible by a mature CMOS process.[18] Conversely, it is difficult to fabricate a light source or an optical amplifier using silicon, which is an indirect bandgap semiconductor. Research on the light emission of silicon has been conducted using Raman amplification,[19] rare earth dope,[20] and quantum effects.[21] However, using III–V compound semiconductors as gain mediums are superior to Si in terms of performance.[22] Therefore, to achieve practical performance, III–V/silicon on insulator (SOI) heterogeneous integrated photonic devices, the so-called hybrid photonic devices have been studied.[23–26] We have also reported a GaInAsP/SOI hybrid laser using a III–V/SOI hybrid gain section and Si waveguide resonators using direct bonding technology.[27–30]

As mentioned earlier, there have been several reports on photonic FPGAs or R-PICs. These PICs consist of only passive elements such as waveguides;[10,11] there are only a few reports of photonic FPGAs that include light sources and active elements. By introducing active elements as reconfigurable elements, circuit design has become sufficiently flexible to realize various applications. We proposed the introduction of a multiple purpose active element that could switch the SOA operation with a laser, consisting of a III–V/SOI hybrid gain section and a reflectivity tunable mirror using a silicon waveguide at both the ends of the gain region. A brief performance of the fabricated reflectivity tunable mirror has been reported.[31]

In this paper, we report the principle, design, and measurement results as well as a comparison between theoretical calculations and the measurement results of a reflectivity tunable reflectivity tunable mirror. In Chapter 2, the operation principle and design of the reflectivity tunable mirror are explained. In Chapter 3, the fabrication and measurement results are presented. In Chapter 4, the comparison between the calculation and measurement results are carried out.

2. Operation principle and design of reflectivity tunable mirror

The proposed reflectivity tunable mirror consists of an MZI with directional couplers and a loop waveguide, as shown in Fig. 1. The reflectance of the mirror depends on the branching ratio of the light injected into the two ports of the loop waveguide. The branching ratio is determined by the phase shift of the MZI arms and the coupling ratio of directional couplers of the MZI. The reflectance of the mirror can be calculated using Eqs. (1), (2).

 © 2022 The Japan Society of Applied Physics

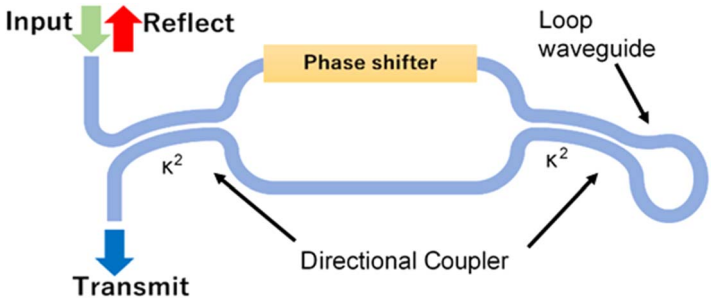

Fig. 1. (Color online) Schematic of reflectivity tunable mirror.

$$\begin{pmatrix} b_1 \\ b_2 \end{pmatrix} = \begin{pmatrix} t_1 & j\kappa_1 \\ j\kappa_1^* & t_1^* \end{pmatrix} \times \begin{pmatrix} \exp j(\beta L_{\mathrm{arm}} + \Delta\phi) & 0 \\ 0 & \exp j\beta L_{\mathrm{arm}} \end{pmatrix} \times \begin{pmatrix} t_2 & j\kappa_2 \\ j\kappa_2^* & t_2^* \end{pmatrix} \begin{pmatrix} 0 & \exp j\beta L_{\mathrm{ring}} \\ \exp j\beta L_{\mathrm{ring}} & 0 \end{pmatrix}$$

$$\begin{pmatrix} t_2 & j\kappa_2 \\ j\kappa_2^* & t_2^* \end{pmatrix} \begin{pmatrix} \exp j(\beta L_{\mathrm{arm}} + \Delta\phi) & 0 \\ 0 & \exp j\beta L_{\mathrm{arm}} \end{pmatrix} \times \begin{pmatrix} t_1 & j\kappa_1 \\ j\kappa_1^* & t_1^* \end{pmatrix} \begin{pmatrix} a_1 \\ 0 \end{pmatrix} \quad (1)$$

$$\text{Reflectance [dB]} = 10\log_{10}\left(\frac{b_1}{a_1}\right)^2. \quad (2)$$

In this equation, a_1, b_1 and b_2 indicate the amplitudes of the electric field, κ_1, κ_2 indicate the directional coupler's coupling coefficient of the electric field, and t_1, t_2 indicate the transmission coefficient of the electric field. L_{ring} and L_{arm} are the lengths of the loop waveguide and MZI's arm, respectively. And $\Delta\phi$ is the phase shift of the MZI arm.

Figure 2 shows the phase shift dependence of the reflectance for each coupling coefficient of the directional coupler. The coupling coefficients of the two couplers should be equal to obtain a reflectivity change from 0 to 1. Therefore, it should satisfy the equation of $\kappa: = \kappa_1 = \kappa_2$ in the following discussion. For the phase shift of π, minimum reflectivity of 0. When κ^2 equals 0.5, the required amount of phase shift is $\pi/2$ for tuning the reflectivity from low to high. When κ^2 equals 0.15, the required amount of phase shift is π. In terms of power consumption for tuning, κ^2 of 0.5, is useful. In terms of controllability (control tolerance), κ^2 of 0.15 is useful.

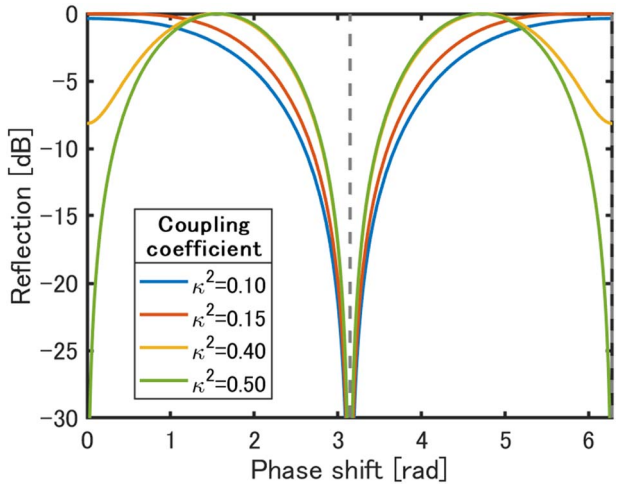

Fig. 2. (Color online) Phase shift dependence of reflectivity tunable mirror.

Figure 3 shows the simulation result of the wavelength dependence of the mirror with κ^2 of 0.5. This simulation contains the wavelength dependence of the directional coupler, which affects most of the dependence of the mirror. In the simulation, the directional coupler had a waveguide width of 500 nm, a rib height of 180 nm a total thickness of 220 nm, a coupling length of 12 μm, and a waveguides gap of 200 nm with a gap etching depth of 130 nm. Our group used a rib waveguide with a thin remaining Si layer to obtain a hydrophobic surface for wafer bonding.[28] The hydrophobic surface is preferable to have a good bonding interface without water void for III–V/Si heterogeneous integration as our final target of hybrid lasers. Since we only have a thickness of 30 nm, the design can be applicable with small modification for conventional channel waveguide.

The gap etching depth is shallower because of the emulating dry etching loading effect for actual fabrication. The wavelength dependence of the directional coupler was calculated by FDTD followed by the wavelength dependence calculation of the whole mirror using a transfer matrix including the calculation results of the directional coupler.[32] The wavelength dependence was relatively small in the entire C-band. For example, when the phase shift is $\pi/4$, the deviation of the reflection is about 0.6 dB within the C-band. When the phase shift is π, the theoretical reflection is completely zero with any κ^2. Therefore, it is not shown in Fig. 3.

3. Fabrication and measurement

3.1. Fabrication

The reflectivity tunable mirror was realized using a single etching process for Si patterning and metal deposition for the micro heater and electrode. The waveguides were fabricated on an SOI chip by utilizing electron beam lithography with proximity effect correction[33] and inductively coupled plasma reactive ion etching with a CF4/SF6 gas mixture. The etching time was determined by the height of the Si rib waveguide. Next, the SiO_2 cladding layer was deposited by a plasma enhanced chemical vapor deposition. After depositing the SiO_2 cladding layer, heater, and electrode patterns were formed. Figure 4(a) shows the circuit design of the fabricated chip. The chip has the mirror section explained above and an

© 2022 The Japan Society of Applied Physics

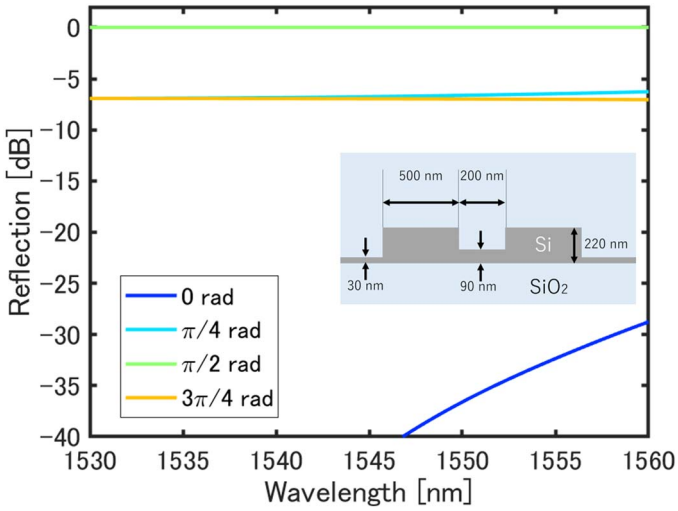

Fig. 3. (Color online) Wavelength dependence of simulation's spectrum of reflection and model of directional.

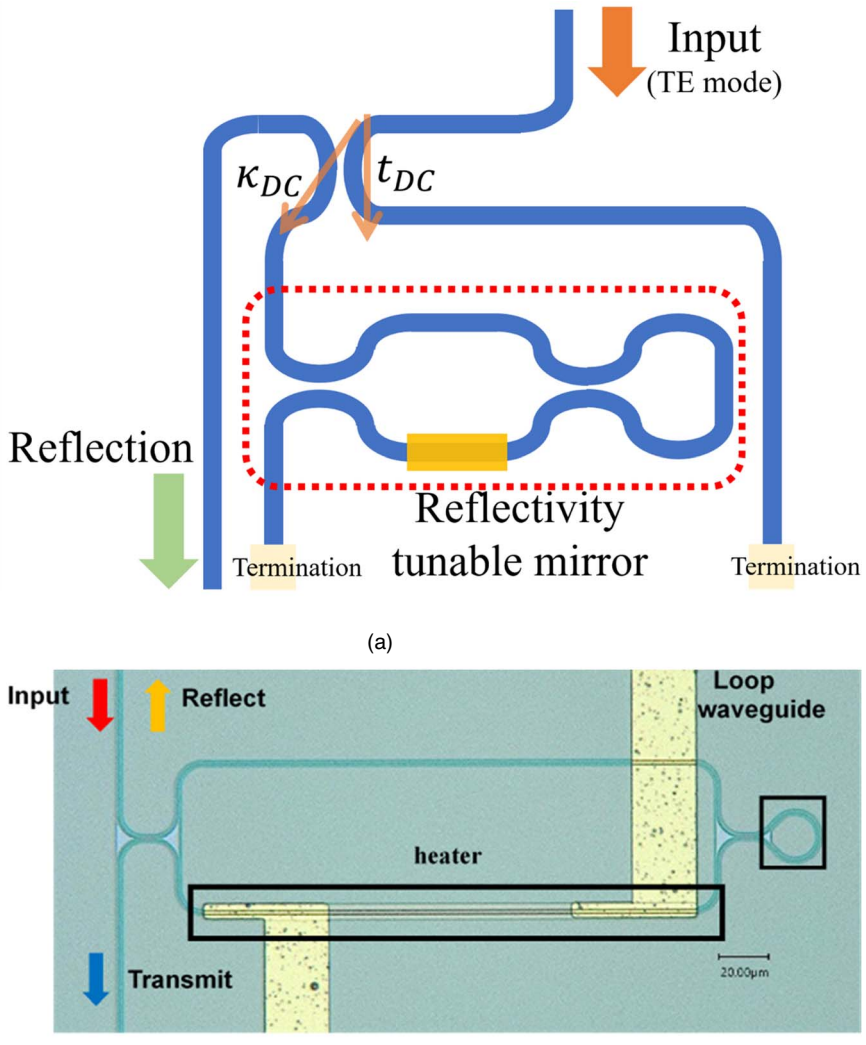

(a)

(b)

Fig. 4. (Color online) (a) Circuit design of the fabricated chip. (b) Microscopic image of the mirror in the chip.

additional 3 dB coupler for reflection power measurement. The width, mesa height and rib thickness of the waveguides were 500 nm, 190 nm, and 30 nm, respectively. The directional coupler was designed for a 3 dB coupler. The gap between of the two waveguides was 200 nm for the 3 dB coupler and MZI's couplers. The arm length of the MZI was 200 μm. The heater was made of 50 nm thick Ti, which had a resistance of 1 kΩ, and the electrode was made of Ti/Au. Light was coupled from the facets with inverse tapered spot size convertors without an AR coating. The coupling length

© 2022 The Japan Society of Applied Physics

of the directional couplers in the mirror was determined for the target coupling coefficient. The design parameter of the reflectivity tunable mirror is κ^2, which is the coupling coefficient of the directional coupler in the MZI. In this work, two target values ($\kappa^2 = 0.5,\ 0.15$) were chosen with a conventional straight directional coupler (SDC) and a curved directional coupler (CDC), which should have better wavelength dependence.[34)]

Figure 4(b) shows a microscopic image of the fabricated mirror, which is part of the circuit shown in Fig. 4(a). In the measurement, the input light was polarized to the TE mode and injected into the Si waveguide via a lensed fiber. The light goes to the mirror through a 3 dB coupler and the reflected power is output from the reflection port.

3.2. Measurement

We measured the mirror with SDC (Device A: $\kappa^2 = 0.47$) and CDC (Device B: $\kappa^2 = 0.10$). Figures 5(a) and 5(b) show the reflection spectra of the fabricated mirrors of Devices A and B, respectively. Please note that the reflection value in Fig. 5 does not show the absolute reflection of the mirror because the value included twice the coupling loss from/to fibers and the waveguide loss outside of the mirror. The plots are moving average in the range of 0.3 nm to remove the ripples from facet reflection. For Device A, by changing the voltage applied to the heater of MZI, the reflection power can change more than 20 dB at 1550 nm. And the deviation of the reflection in C-band was about 3.1 dB at 0 V. For Device B, by changing the voltage applied to the heater of MZI, the reflection power can change more than 16 dB at 1550 nm. The deviation of the reflection in the C-band was approximately 1.8 dB at 0 V. This wavelength dependence reflected the characteristics of the coupling coefficient κ^2 of the directional coupler, which are shown in Fig. 6 for Device A. This coupling coefficient was obtained by measuring the test directional coupler fabricated on the same chip. The value was varied from 0.42 to 0.53 for the entire range of C-band.

4. Discussion

In this chapter, a comparison between the measurement and theory is discussed. As discussed in Sect. 2, Eqs. (1) and (2) are theoretical equations. In actual measurements, for example, the amount of phase shift is unknown. This is because phase shift was obtained by applying voltage. Therefore, assuming that the amount of phase shift is proportional to the square of the applied voltage, the phase shift $\Delta\phi$ can be expressed as:

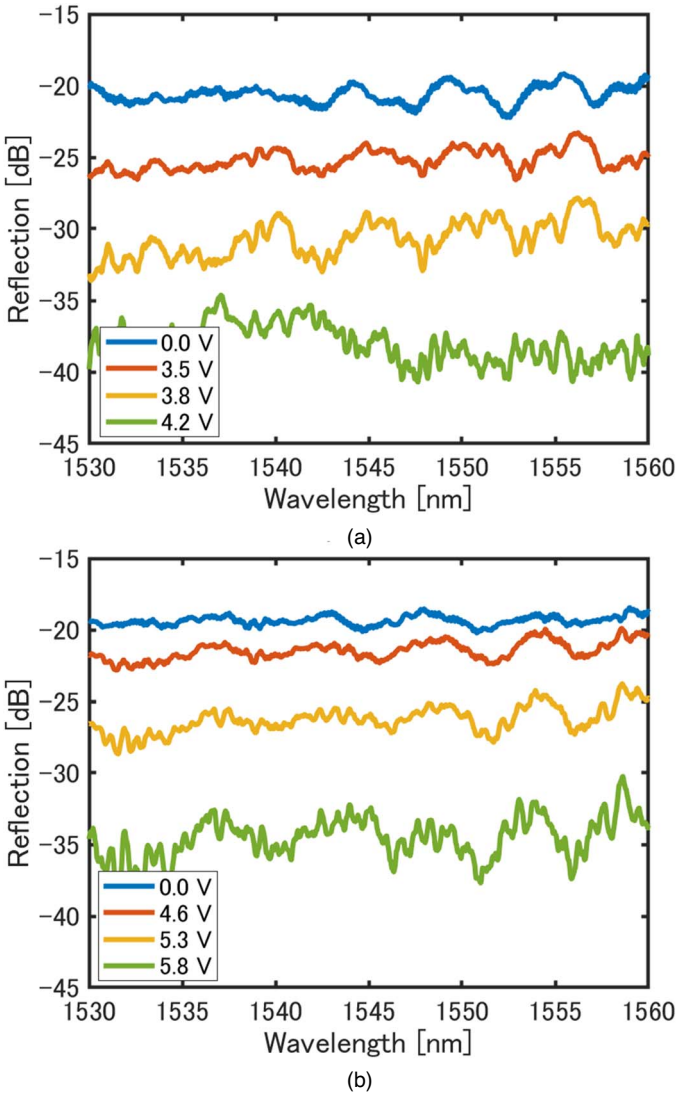

Fig. 5. (Color online) Spectrum of mirror's reflection for each applied voltage. The directional coupler's kappa is shown in Fig. 6.

© 2022 The Japan Society of Applied Physics

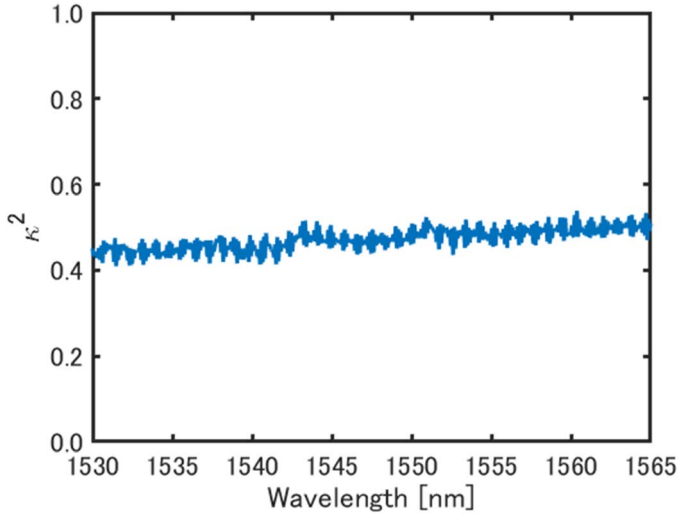

Fig. 6. (Color online) Spectrum of kappa of the mirror's directional coupler.

$$\Delta\phi = \alpha_{v2\mathrm{phi}} V^2 + \phi_{\mathrm{init}}, \tag{3}$$

where $\alpha_{v2\mathrm{phi}}$ indicates a constant of proportional, ϕ_{init} indicates an initial phase shift, and V indicates applied voltage. In the measurement, there was a loss in the waveguides and background bias power. By including the two parameters, Eq. (2) can be replaced by Eq. (4)

$$\text{Reflectance [dB]} = 10\log_{10}\left(\left(\frac{b_1}{a_1}\right)^2 + \text{bias}\right) + \text{loss}. \tag{4}$$

From Eqs. (1), (3), and (4) and measurement data, the values of four unknown parameters obtained by parameter fitting with least squares method. Figures 7(a), and 7(b) show the applied voltage dependence of reflectivity at 1550 nm for devices A and B, respectively. The horizontal axis is the voltage applied to the heater and the vertical axis is the reflection. Figure 7 shows the fitting curves. For the fittings, we used $\kappa^2 = 0.47$ for Device A and $\kappa^2 = 0.10$ for Device B. The voltage required to turn the reflection on and off differs depending on the difference in κ^2. These plots show that the phase shift dependence of the reflectance of the mirror was determined by the coupling coefficient of the directional coupler. From these fitting parameters, the horizontal axis in Fig. 7 can be converted to a phase shift as shown in Fig. 8. Due to the initial phase shift caused by small asymmetricity, measurement point did not start from 0 rad at an applied voltage of 0 V. The theoretical curves are shown in Fig. 8. The measurement data and the theory agree well and it shows different characteristics by the different design of the coupling coefficient κ^2. By appropriately setting κ^2, the amount of phase shift required to change the reflectance of the mirror can be changed, so that the sensitivity of the reflectance due to the phase shift can be controlled.

5. Conclusion

We demonstrated a reflectivity tunable mirror of MZI and a loop waveguide for the reconfigurable PICs. The reflection power can change by more than 20 dB by a phase shift. The characteristic of the reflectivity tunable mirror is determined by κ^2, the coupling coefficient of the directional coupler of the MZI. The amount of phase shift required for the reflection change can be determined using the value of κ^2. The reflection of the mirror with a directional coupler of $\kappa^2 = 0.47$ can change by 20 dB at 1550 nm with a phase

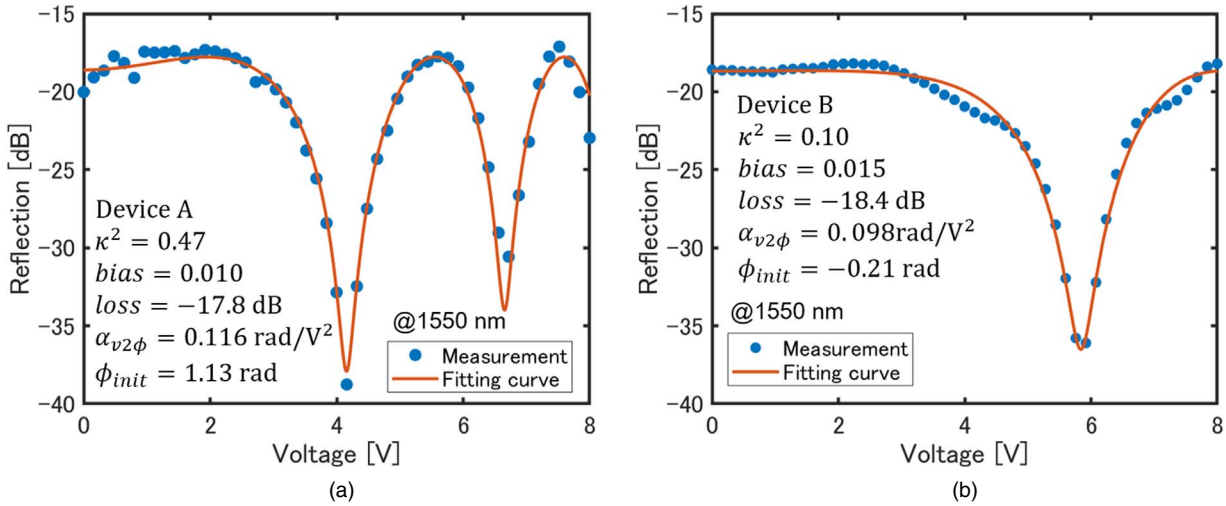

Fig. 7. (Color online) Heater applied voltage dependence of reflectance at 1550 nm. (a) The directional coupler's $\kappa^2 = 0.47$ (b) $\kappa^2 = 0.10$.

© 2022 The Japan Society of Applied Physics

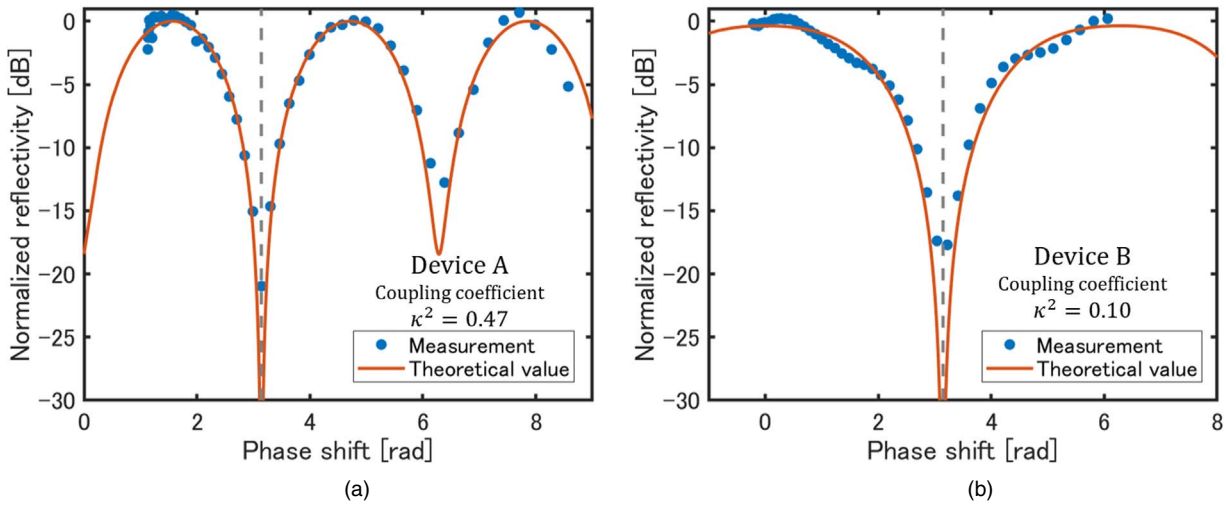

Fig. 8. (Color online) Phase shift dependence of reflectance of the measurement data and theoretical plot at 1550 nm. (a) Directional coupler's $\kappa^2 = 0.47$ (b) $\kappa^2 = 0.10$.

shift of $\pi/2$. The reflection of the mirror with a directional coupler of $\kappa^2 = 0.10$ can change by 16 dB at 1550 nm by a π phase shift. The two devices show that κ^2 is a parameter that determines the mirror's characteristics. The phase shift sensitivity of the reflectance can be controlled by designing κ^2.

Acknowledgments

This work is supported by New Energy and Industrial Technology Development Organization (NEDO) and JST-CREST(JPMJCR15N6).

ORCID iDs

Nobuhiko Nishiyama https://orcid.org/0000-0001-8288-6690

1) R. Soref, IEEE J. Sel. Top. Quantum Electron. **12**, 1678 (2006).
2) X. Chen, M. M. Milosevic, S. Stanković, S. Reynolds, T. D. Bucio, K. Li, D. J. Thomson, F. Gardes, and G. T. Reed, Proc. IEEE **106**, 2101 (2018).
3) N. Nishiyama and S. Arai, Int. Symp. Photonics Electronics Convergence 2015, 2015.
4) B. Wim, European Conf. Integrated Optics 2018, 2018, p. 51.
5) W. Bogaerts, D. Pérez, J. Capmany, D. A. B. Miller, J. Poon, D. Englund, F. Morichetti, and A. Melloni, Nature **586**, 207 (2020).
6) Y. Shen et al., Nat. Photonics **11**, 441 (2017).
7) N. C. Harris et al., Nat. Photonics **11**, 447 (2017).
8) N. C. Harris et al., Optica **5**, 1623 (2018).
9) B. J. Shastri, A. N. Tait, T. F. de Lima, W. H. P. Pernice, H. Bhaskaran, C. D. Wright, and P. R. Prucnal, Nat. Photonics **15**, 102 (2021).
10) J. Carolan et al., Science **349**, 711 (2015).
11) W. Clements, P. Humphreys, B. Metcalf, W. Kolthammer, and I. Walmsley, Optica **3**, 1460 (2016).
12) D. P. López, A. M. Gutierrez, E. Sánchez, P. DasMahapatra, and J. Capmany, Opt. Express **27**, 38071 (2019).
13) P. Daniel, G. Ivana, and C. Jose, Opt. Express **26**, 27265 (2018).
14) L. Zhuang, C. G. H. Roeloffzen, M. Hoekman, K. J. Boller, and A. J. Lowery, Optica **2**, 854 (2015).
15) N. Quack, H. Sattari, A. Y. Takabayashi, Y. Zhang, P. Verheyen, W. Bogaerts, P. Edinger, C. Errando-Herranz, and K. B. Gylfason, IEEE J. Quantum Electron. **56**, 8400210 (2020).
16) C. Errando-Herranz, A. Y. Takabayashi, P. Edinger, H. Sattari, K. B. Gylfason, and N. Quack, IEEE J. Sel. Top. Quantum Electron. **26**, 8200916 (2020).
17) W. Bogaerts et al., Proc. SPIE **11285**, 1128503 (2020).
18) A. Rahim, T. Spuesens, R. Baets, and W. Bogaerts, Proc. IEEE **106**, 2313 (2018).
19) Y. Takahashi, Y. Inui, M. Chihara, T. Asano, R. Terawaki, and S. Noda, Nature **498**, 470 (2013).
20) J. D. B. Bradley and E. S. Hosseini, Opt. Express **22**, 12226 (2014).
21) J. Liu, L. C. Kimerling, and J. Michel, Semicond. Sci. Technol. **27**, 094006 (2012).
22) Z. Fang, Q. Y. Chen, and C. Z. Zhao, Opt. Laser Technol. **46**, 103 (2013).
23) A. W. Fang, H. Park, O. Cohen, R. Jones, M. J. Paniccia, and J. E. Bowers, Opt. Express **14**, 9203 (2006).
24) D. Liang and J. E. Bowers, Light: Adv. Manuf. **2**, 59 (2021).
25) B. Song, C. Stagarescu, S. Ristic, A. Behfar, and J. Klamkin, Opt. Express **24**, 10435 (2016).
26) M. A. Tran, D. Huang, and J. E. Bowers, APL Photonics **4**, 111101 (2019).
27) Y. Hayashi, J. Suzuki, S. Inoue, S. M. T. Hasan, Y. Kuno, K. Itoh, T. Amemiya, N. Nishiyama, and S. Arai, Jpn. J. Appl. Phys. **55**, 082701 (2016).
28) J. Suzuki, F. Tachibana, K. Nagasaka, M. Eissa, L. Bai, T. Mitarai, T. Amemiya, N. Nishiyama, and S. Arai, Jpn. J. Appl. Phys. **57**, 094101 (2018).
29) Y. Wang, K. Nagasaka, T. Mitarai, Y. Ohiso, T. Amemiya, and N. Nishiyama, Jpn. J. Appl. Phys. **59**, 052004 (2020).
30) T. Hiratani, N. Fujiwara, T. Kikuchi, N. Inoue, T. Ishikawa, T. Nitta, M. Eissa, Y. Oiso, N. Nishiyama, and H. Yagi, 27th Int. Semiconductor Laser Conf., 2021.
31) Y. Makihara, M. Eissa, T. Amemiya, and N. Nishiyama, Ext. Abstr. Solid State Devices and Materials, 2021, p. 277.
32) T. Mitarai, M. Eissa, T. Miyazaki, T. Amemiya, and N. Nishiyama, Jpn. J. Appl. Phys. **59**, 112002 (2020).
33) M. Eissa, T. Mitarai, T. Amemiya, Y. Miyamoto, and N. Nishiyama, Jpn. J. Appl. Phys. **59**, 126502 (2020).
34) H. Morino, T. Maruyama, and K. Iiyama, J. Lightwave Technol. **32**, 2188 (2014).

© 2022 The Japan Society of Applied Physics